

Article

Rapid and Sensitive Detection of Influenza B Virus Employing Nanocomposite Spheres Based on Ag-Doped ZnIn₂S₄ Quantum Dots

Jia-Xuan Hu, Li-Bang Zhu, Sheng-Tong Wu  and Shou-Nian Ding * 

Jiangsu Province Hi-Tech Key Laboratory for Bio-Medical Research, School of Chemistry and Chemical Engineering, Southeast University, Nanjing 211189, China; 220213216@seu.edu.cn (J.-X.H.)

* Correspondence: snding@seu.edu.cn; Fax: +86-25-52090621

Abstract: Lateral flow immunoassay (LFIA) technology serves a significant role as a simple and rapid biosensor in the detection of influenza viruses. The focus of this study is the development of a rapid and convenient screening method for influenza B virus (IBV) proteins using a fluorescence lateral flow biosensor based on Ag-doped ZnIn₂S₄ quantum dots (Ag: ZIS QDs) as signal reporters. These Ag: ZIS QDs-emitting orange fluorescence are loaded onto dendritic mesoporous silica nanoparticles (DMSNs) and are further coated with a layer of silica shell to form a core-shell structured composite nanomaterial (SiO₂ @ Ag: ZIS QDs @ DMSNs). The orange fluorescence effectively eliminates the interference of blue background fluorescence, significantly enhancing the detection sensitivity. This technology demonstrates outstanding performance in the immediate detection of IBV, with a minimum detection limit of 1 ng/mL, compared to the traditional colloidal gold strip with a detection limit of 6 ng/mL. Furthermore, both intra-assay and inter-assay coefficients of variation (CV) are less than 9%. This method holds promise for wide application in early diagnosis, epidemiological investigation, and epidemic surveillance of IBV.

Keywords: influenza B virus; lateral flow immunoassay; Ag-doped ZnIn₂S₄ QDs; dendritic silica



Citation: Hu, J.-X.; Zhu, L.-B.; Wu, S.-T.; Ding, S.-N. Rapid and Sensitive Detection of Influenza B Virus Employing Nanocomposite Spheres Based on Ag-Doped ZnIn₂S₄ Quantum Dots. *Chemosensors* **2024**, *12*, 68. <https://doi.org/10.3390/chemosensors12040068>

Received: 19 March 2024

Revised: 16 April 2024

Accepted: 17 April 2024

Published: 19 April 2024



Copyright: © 2024 by the authors. Licensee MDPI, Basel, Switzerland. This article is an open access article distributed under the terms and conditions of the Creative Commons Attribution (CC BY) license (<https://creativecommons.org/licenses/by/4.0/>).

1. Introduction

Influenza B Virus (IBV) is a significant respiratory pathogen capable of inducing respiratory infection, ranging from mild symptoms to severe pneumonia. The global incidence of IBV cases remains consistently high throughout the year [1–3]. Hence, the rapid and precise detection of IBV is paramount for influenza prevention, early diagnosis, and timely treatment, as immediate virus detection can substantially mitigate transmission at the source [4,5]. Presently, the primary methods for detecting infectious disease pathogens involve nucleic acid and antigen testing [6]. Polymerase chain reaction (PCR), the most commonly utilized nucleic acid testing method, provides high sensitivity and specificity [7]. However, its implementation demands specialized personnel, dedicated equipment, and laboratory facilities, making it time-consuming and challenging to achieve rapid and real-time virus detection [8]. Antigen testing is an immunological analysis method grounded in the antigen–antibody reaction. Conventional antigen analysis techniques, such as enzyme-linked immunosorbent assay (ELISA) [9], entail intricate procedures, strict operational control, and relatively lower detection accuracy. Surface-enhanced Raman spectroscopy (SERS) [10] involves a lengthier detection period and substantial testing costs. In contrast, lateral flow immunoassay (LFIA) emerges as a simple, swift, sensitive, and cost-effective method, positioning it as one of the most widely employed point-of-care testing (POCT) sensors [11]. In IBV detection, LFIA exhibits the potential to furnish rapid and accurate outcomes by targeting the virus’s protein antigen [12]. The judicious selection of markers is pivotal in augmenting sensitivity in this context.

In recent years, colloidal gold test strips have become the predominant LFIA in the market, yielding visually discernible results [13–16]. However, significant batch-to-batch variations in colloidal gold products have led to a compromise in sensitivity. The physical adsorption method, often used in conjunction, frequently detaches antibodies from the gold particle surface, introducing instability to the labeled markers [17]. Quantum Dots (QDs) have emerged as innovative fluorescent labels in the biomedical field, presenting advantages such as narrow fluorescence emission peaks, extended lifetimes, and high fluorescence quantum yields, rendering them ideal biomarkers [18–20]. Integrating QDs with LFIA and utilizing them as labeled antibodies amplifies sensitivity and stability in detection and enables the simultaneous identification of multiple markers, facilitating multifactorial analysis [21–25]. However, in practical applications, quantum dots often encounter luminescence quenching effects induced by aggregation [26]. The construction of composite materials through integrating quantum dots with other functional materials, such as silica and polystyrene nanoparticles, enhances biocompatibility and fluorescence stability [27–31]. This strategy mitigates the quenching of QDs fluorescence while concurrently amplifying the signal, significantly enhancing detection sensitivity and specificity. Li et al. successfully established a highly sensitive immunoassay, termed quantum dot-linked immunosorbent assay (QLISA), for the detection of C-reactive protein (CRP) by surface-conjugating CdSe/ZnS core/shell QDs onto silica microspheres, achieving a low detection limit (LOD) of 0.32 ng/mL [28]. Additionally, Li et al. facilely loaded quantum dots onto the surface of polystyrene (PS) nanoparticles using polyelectrolytes and applied them in suspension chip detection for the H5N1 virus, demonstrating a sensitivity lower than 25 PFU/mL [30]. In comparison to dense silica and polystyrene spheres, dendritic mesoporous silica nanoparticles (DMSNs) possess expanded radial pore structures and an ultra-large specific surface area. Utilizing DMSNs as carriers not only enables the attachment of more quantum dots, ensuring stable luminescence, but also amplifies the signal [32,33].

Herein, we utilized orange fluorescent QDs loaded onto DMSNs (SiO₂ @ Ag: ZIS QDs @ DMSNs) as the signal reporting entity. Harnessing the simplicity of a lateral flow detection platform, we designed a straightforward one-step fluorescent lateral flow biosensor to screen IBV proteins rapidly. The detection limit achieved was 1 ng/mL, representing a six-fold reduction compared to previously reported colloidal gold test strips [4]. This technology exhibits broad potential applications for the early diagnosis of IBV, epidemiological investigations, and pandemic monitoring. Moreover, the technology platform based on SiO₂ @ Ag: ZIS QDs @ DMSNs demonstrates remarkable sensitivity, and can be readily applied to the routine diagnostic testing of acute infectious diseases (such as procalcitonin, HIV, syphilis, hepatitis, etc.) and common tumor markers (AFP, CA199, CEA, etc.). This is expected to make significant advancements in healthcare and epidemiology.

2. Materials and Methods

2.1. Reagents

Indium (III) nitrate, cetyltrimethyl ammonium bromide (CTAB), sodium salicylate, ammonia, triethanolamine, sulfur powder, NaCl, Tween-20, γ -aminopropyltriethoxysilane (APTES), thioacetamide (TAA), succinic anhydride, Na₂HPO₄, NaH₂PO₄, tetraethyl orthosilicate (TEOS), concentrated hydrochloric acid (HCl), silver nitrate, polyvinyl pyrrolidone (PVP), L-cysteine, zinc acetate, N, N-Dimethylformamide (DMF), absolute ethanol, and NaOH were obtained from Sinopharm Chemical Reagent Co., Ltd. (Shanghai, China). All chemicals were used as received without purification. Bovine serum albumin (BSA) was sourced from Sangon Biotech Co., Ltd. (Shanghai, China). The absorbent pad, nitrocellulose (NC) membrane, sample pad, goat anti-mouse IgG antibody, Zika NS1 recombinant protein, HCG antigen, and polyvinyl chloride (PVC) substrate were acquired from Shanghai Jieyi Biotechnology Co., Ltd. (Shanghai, China). Prepare phosphate-buffered saline (PBS, 0.01 M, pH 7.4) using Na₂HPO₄ and NaH₂PO₄. Alpha-fetoprotein (AFP) antigen was purchased from Shanghai Linc-Bio Science Co., Ltd. (Shanghai, China). The Jiangsu Provincial Center

for Disease Control and Prevention provides recombinant nucleoprotein of IBV and its matching labeled antibody and coated antibody. Chemical Co., Ltd. (Shanghai, China) supplied 1-(3-Dimethylaminopropyl)-3-ethylcarbodiimide hydrochloride (EDC).

2.2. Preparation of Ag-Doped ZnIn₂S₄ Quantum Dots (Ag: ZIS QDs)

The synthesis of Ag: ZIS QDs was carried out through a hydrothermal process [34]. A precursor solution was prepared by dissolving 226.3 mg of zinc acetate and 870.1 mg of indium (III) acetate in 70 mL of deionized water. Subsequently, 565.8 mg of silver nitrate was introduced into this solution to initiate the formation of Ag: ZIS QDs. Then, a solution containing 26.3 mg of L-cysteine was added with vigorous stirring, followed by the adjustment of the pH to 8.5 using a 1.0 M NaOH solution. Immediately after, an excess amount of TAA (1.05 g) was quickly mixed into the solution. The resulting mixture was sealed in a polytetrafluoroethylene-lined hydrothermal autoclave and heated to 110 °C for a duration of 4 h. After cooling back to room temperature, the Ag: ZIS QDs were separated by centrifugation at 10,000 rpm for 30 min. Subsequently, they were washed three times by centrifugation with a solution composed of water and ethanol in a 30:70 volume ratio. Finally, the purified QDs were dispersed in 50 mL of deionized water.

2.3. Preparation of SiO₂ @ Ag:ZIS QDs @ DMSNs

The preparation of DMSNs and their surface modification was carried out using the previously reported method [35]. Specifically, 10 mg of prepared DMSNs was dispersed in 10 mL of ethanol. To this, 200 µL of ammonia solution and 40 µL of APTES were added to react with surface silanol groups, resulting in the DMSNs surface modification with -NH₂ groups. The mixture was stirred at room temperature for 12 h. The resulting product was collected by centrifugation and washed three times with ethanol. Finally, the obtained amine-functionalized DMSNs were dispersed in 10 mL of deionized water. The aforementioned DMSNs were then dispersed in different volumes of Ag: ZIS QDs water solution and a 10 mg solution of EDC. The solution was stirred for 6 h, followed by centrifugation at 10,000 rpm for 5 min to remove unbound quantum dots. The Ag: ZIS QDs @ DMSNs nanospheres were washed twice with deionized water through centrifugation and dispersed in 10 mL of deionized water. Subsequently, the Ag: ZIS QDs @ DMSNs nanospheres were dispersed in 4 mL of ethanol, and 10 µL of TEOS was added, followed by stirring for 24 h. The SiO₂ @ Ag: ZIS QDs @ DMSNs nanospheres were collected by centrifugation, washed three times with ethanol, and dispersed in 10 mL of ethanol.

2.4. Preparation of SiO₂ @ Ag:ZIS QDs @ DMSNs-IVB Antibody

The procedure involved reacting a 10 mL ethanol solution of SiO₂ @ Ag: ZIS QDs @ DMSNs (1 mg/mL) with 200 µL of ammonia solution and 40 µL of APTES. The mixture was stirred at room temperature for 6 h, followed by centrifugation at 8000 rpm for 5 min and washing with anhydrous ethanol twice to obtain SiO₂ @ Ag: ZIS QDs @ DMSNs-NH₂. The resulting product was then dispersed in 10 mL of DMF. Subsequently, 100 mg of succinic anhydride was added, and the mixture was stirred at room temperature for 4 h. After centrifugation and washing, carboxyl-terminated SiO₂ @ Ag: ZIS QDs @ DMSNs were obtained. Following this, 0.25 mL of SiO₂ @ Ag: ZIS QDs @ DMSNs-COOH (1 mg/mL), 20 µL of EDC water solution (10 mg/mL), and IBV labeled antibody (IBV-Ab₂, 10.4 mg/mL) were sequentially mixed thoroughly. The mixture was gently shaken at room temperature for 2 h. The resulting product was centrifuged and dispersed in 0.25 mL of 0.01 M PBS solution, stored at 4 °C.

2.5. Detection of SiO₂ @ Ag:ZIS QDs @ DMSNs-LFIA

The sample pad was treated with a mixed solution containing 0.1% Tween-20, 1% BSA, and 4% NaCl, followed by air-drying at room temperature. Using a line pen, IBV capture antibody (IBV-Ab₁, 2 mg/mL) and goat anti-mouse IgG antibody (2 mg/mL) were, respectively, applied to the test and control line on the NC membrane, followed by air-drying

at room temperature. Subsequently, the absorbent pad, NC membrane, and pre-treated sample pad were adhered to a PVC backing card, cut into 4 mm wide strips, and stored at 4 °C in the dark. The Antigen-IBV standard solution was diluted to different concentrations with 0.01 M PBS solution. Then, 10 μL $\text{SiO}_2 @ \text{Ag: ZIS QDs @ DMSNs-antibody}$ (IBV-Ab_2) was mixed with 30 μL of the Antigen-IBV standard solution of different concentrations, and the mixture was dropped onto the sample pad. After a 10 min incubation period, fluorescent images of the test paper were captured using a Huawei smartphone under a 365 nm UV lamp. The fluorescence intensity of the control and test lines was analyzed using ImageJ software (ImageJ 1.53t).

3. Results and Discussion

3.1. Characterization of $\text{SiO}_2 @ \text{Ag: ZIS QDs @ DMSNs}$

Figure 1 illustrates the complete process of preparing $\text{Ag: ZIS QDs @ DMSNs}$ nanocomposite materials. Preliminary analysis of the microstructure of the products at each stage was conducted using Transmission Electron Microscopy (TEM) and Scanning Electron Microscopy (SEM). Figures 2a and S1a present the TEM images of DMSNs, showing particle sizes ranging from 220 to 250 nm with large pore sizes, indicating the excellent loading capacity of DMSNs. Figures 2b and S1b depict the TEM images of $\text{Ag: ZIS QDs @ DMSNs}$ nanocomposite materials, clearly revealing the firm attachment of Ag: ZIS QDs to DMSNs, demonstrating the successful preparation of the composite material. The TEM images in Figures 2c and S1c clearly illustrate the successful encapsulation of SiO_2 on the surface of $\text{Ag: ZIS QDs @ DMSNs}$, preventing the detachment of Ag: ZIS QDs and resulting in a decrease in the fluorescence intensity of the composite material, while simultaneously enhancing its stability in acidic and alkaline environments. EDS elemental mapping indicates that $\text{Ag: ZIS QDs @ DMSNs}$ are composed of Si, O, Ag, Zn, In, and S elements (Figures 2d–i and S1d), confirming the successful loading of QDs. Elemental mapping shows the distribution of Zn (green), In (purple), S (orange), and Ag (yellow) elements around the Si (blue) and O (red) atomic cores.

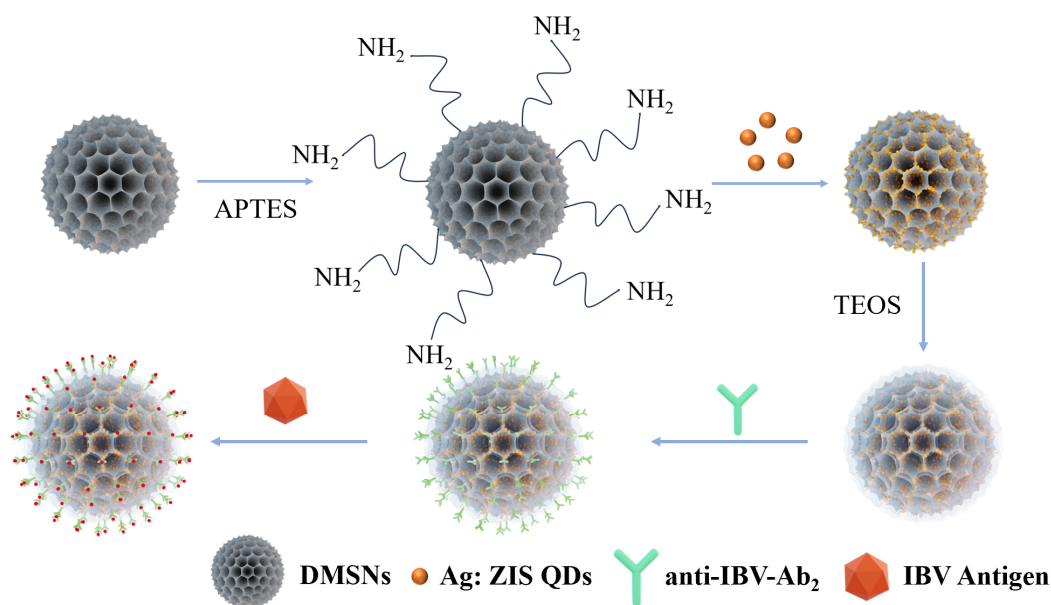


Figure 1. Synthesis process diagram of $\text{SiO}_2 @ \text{Ag: ZIS QDs @ DMSNs}$.

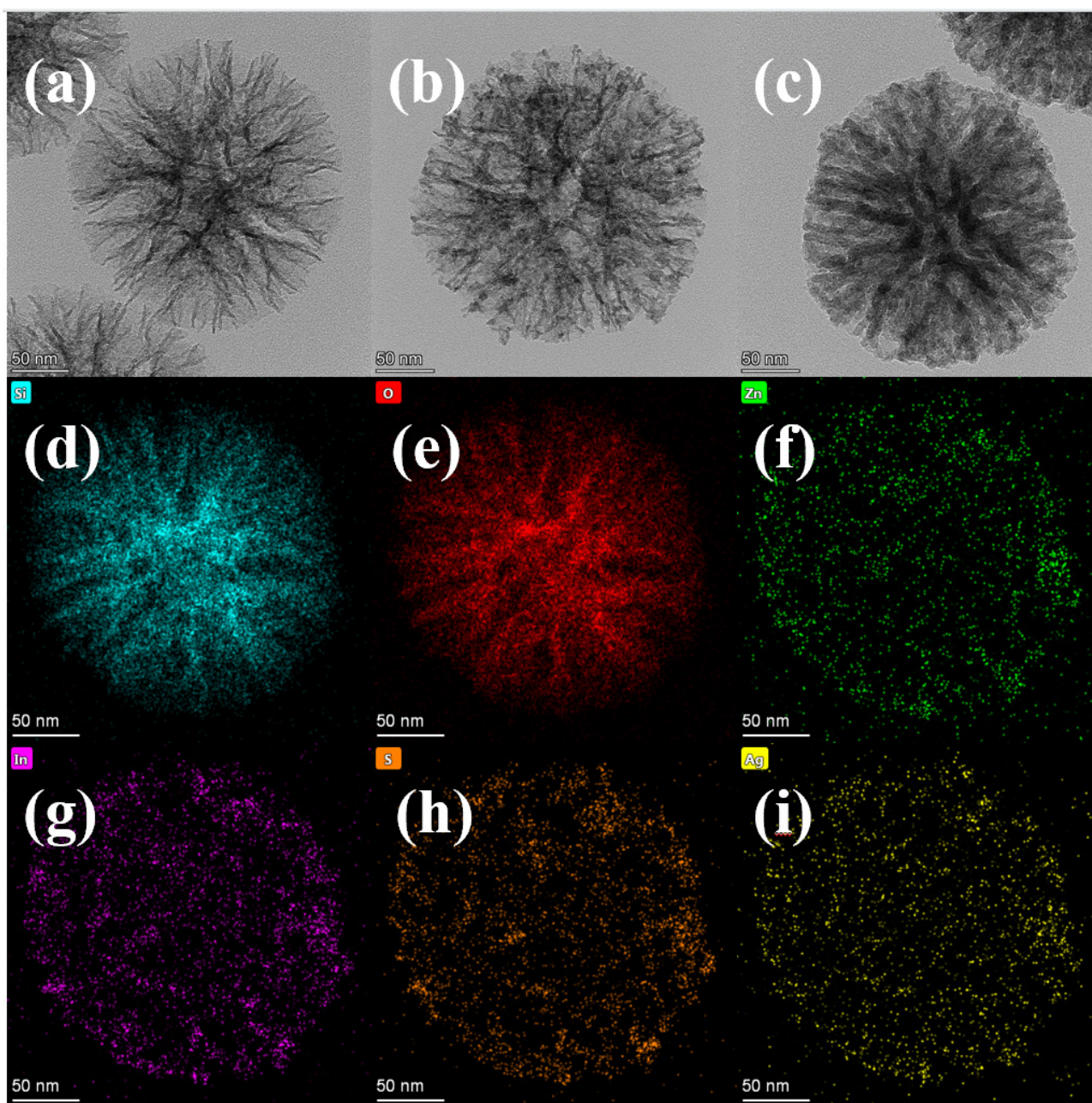


Figure 2. (a) TEM images of DMSNs; (b) TEM image of Ag: ZIS QDs @ DMSNs; (c) TEM image of SiO₂ @ Ag: ZIS QDs @ DMSNs; (d–i) EDS mapping images of SiO₂ @ Ag: ZIS QDs @ DMSNs.

The high-resolution transmission electron microscopy (HRTEM) image of Ag-ZIS quantum dots is depicted in Figure 3a, clearly revealing their uniform size distribution within the range of 5–10 nm and indicating the absence of aggregation. Additionally, Figure 3b shows an obvious lattice fringe, with an arrow pointing to a lattice spacing of 0.325 nm, precisely aligned with the (102) crystal lattice plane of hexagonal ZnIn₂S₄ [36].

We conducted a comprehensive analysis of the composition of SiO₂ @ Ag: ZIS QDs @ DMSNs using X-ray diffraction (XRD), Fourier-transform infrared (FT-IR) spectroscopy, ultraviolet-visible absorption (UV-vis), and fluorescence spectroscopy. Figure 4a presents the XRD spectra of DMSNs and SiO₂ @ Ag: ZIS QDs @ DMSNs. The diffraction broad peak observed at 22° for DMSNs aligns with the diffraction peak of the SiO₂ standard card (ICDD JCPDS card No. 39-1425), confirming the successful preparation of DMSNs. The XRD pattern of SiO₂ @ Ag: ZIS QDs @ DMSNs exhibits characteristic peaks corresponding

to the (101) crystal plane of SiO_2 and the (008), (112), and (203) crystal planes of hexagonal ZnIn_2S_4 , matching with the diffraction peaks of the ZnIn_2S_4 standard card (ICDD JCPDS card No. 72-0773), further confirming the successful loading of Ag: ZIS QDs [36]. Figure 4b presents the FT-IR spectra, showing the stretching characteristic peak of Si-O-Si at 1088 cm^{-1} and peaks at 955 and 794 cm^{-1} corresponding to the Si-O-H feature peaks. For SiO_2 @ Ag: ZIS QDs @ DMSNs, features such as O-H (3430 cm^{-1}), $-\text{CH}_2$ ($2918, 2850\text{ cm}^{-1}$), C-O (1657 cm^{-1}), C-C (1564 cm^{-1}), and C-H (1383 cm^{-1}) are observed, while the Si- CH_2 (806 cm^{-1}) characteristic peak disappears. This may be attributed to the forming of SiO_2 film on the surface of Ag: ZIS QDs @ DMSNs, causing the disappearance of the Si- CH_2 . Additionally, the robust and broad absorption band in the $900\text{--}1300\text{ cm}^{-1}$ range is attributed to C-C, Si-O, and C-O/C-N. The broadening of the peaks in this range is due to the formation of hydrogen bonds between SiO_2 @ Ag: ZIS QDs @ DMSNs molecules. The UV-Vis absorption spectra in Figure 4c show an absorption peak at approximately 290 nm for SiO_2 @ Ag: ZIS QDs @ DMSNs with concentrations of 0.1 mg/mL , further confirming the successful loading of QDs. Figure 4d shows the fluorescence spectrum of SiO_2 @ Ag: ZIS QDs @ DMSNs, exhibiting an emission wavelength of 600 nm under the optimal excitation wavelength of 300 nm . DMSNs themselves are non-fluorescent, and the successful loading of QDs imparts fluorescence to the composite material, making it suitable for applications in the field of immunochromatographic analysis. The zeta potential is an independent method to evaluate the stability of nanoparticles (Figure 4e). The zeta potential of DMSNs indicates a negative surface charge of -21.89 mV . The presence of quantum dots on the silica spheres causes a change in the zeta potential to -19.37 mV , suggesting relative instability of Ag: ZIS QDs @ DMSNs. This could be due to hindered loading efficiency, likely caused by spatial hindrance. Carboxylation reactions of hydrophilic quantum dots with residual amino groups on the surface of DMSNs reduce the zeta potential of Ag: ZIS QDs @ DMSNs. The zeta potential of SiO_2 @ Ag: ZIS QDs @ DMSNs is -21.18 mV , almost identical to that of the silica spheres, indicating successful encapsulation with an outer silica layer. The zeta potential of amine-functionalized SiO_2 @ Ag: ZIS QDs @ DMSNs is 14.11 mV , while carboxyl-functionalized SiO_2 @ Ag: ZIS QDs @ DMSNs has a zeta potential of -37.09 mV , demonstrating that hydrophilic layer encapsulation significantly improves the stability of SiO_2 @ Ag: ZIS QDs @ DMSNs in water.

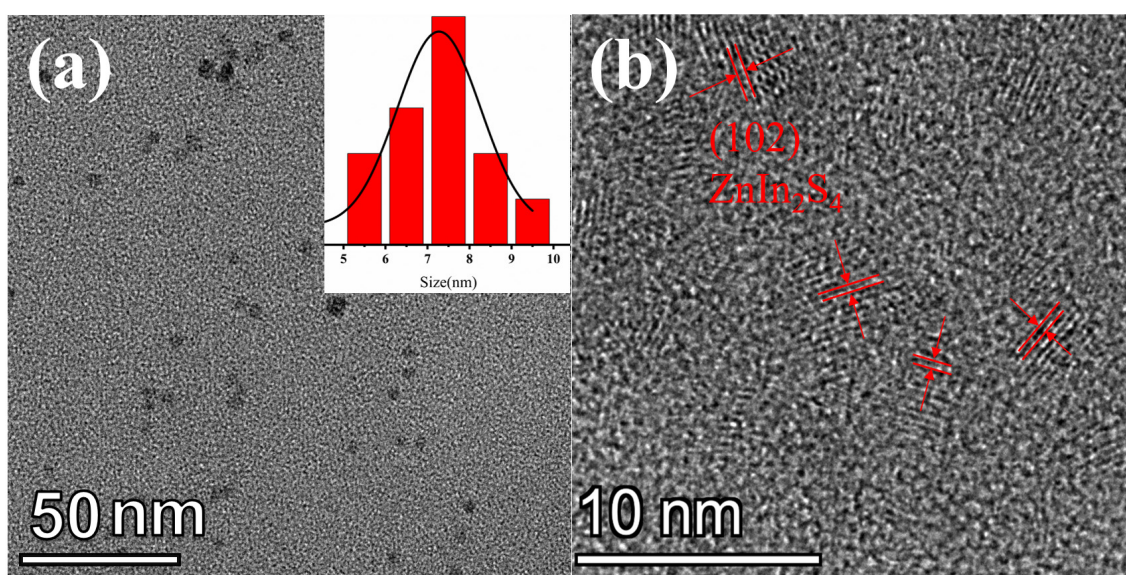


Figure 3. (a) TEM image of Ag: ZIS QDs and the corresponding particle size distribution (inset); (b) the lattice stripe image of Ag: ZIS QDs.

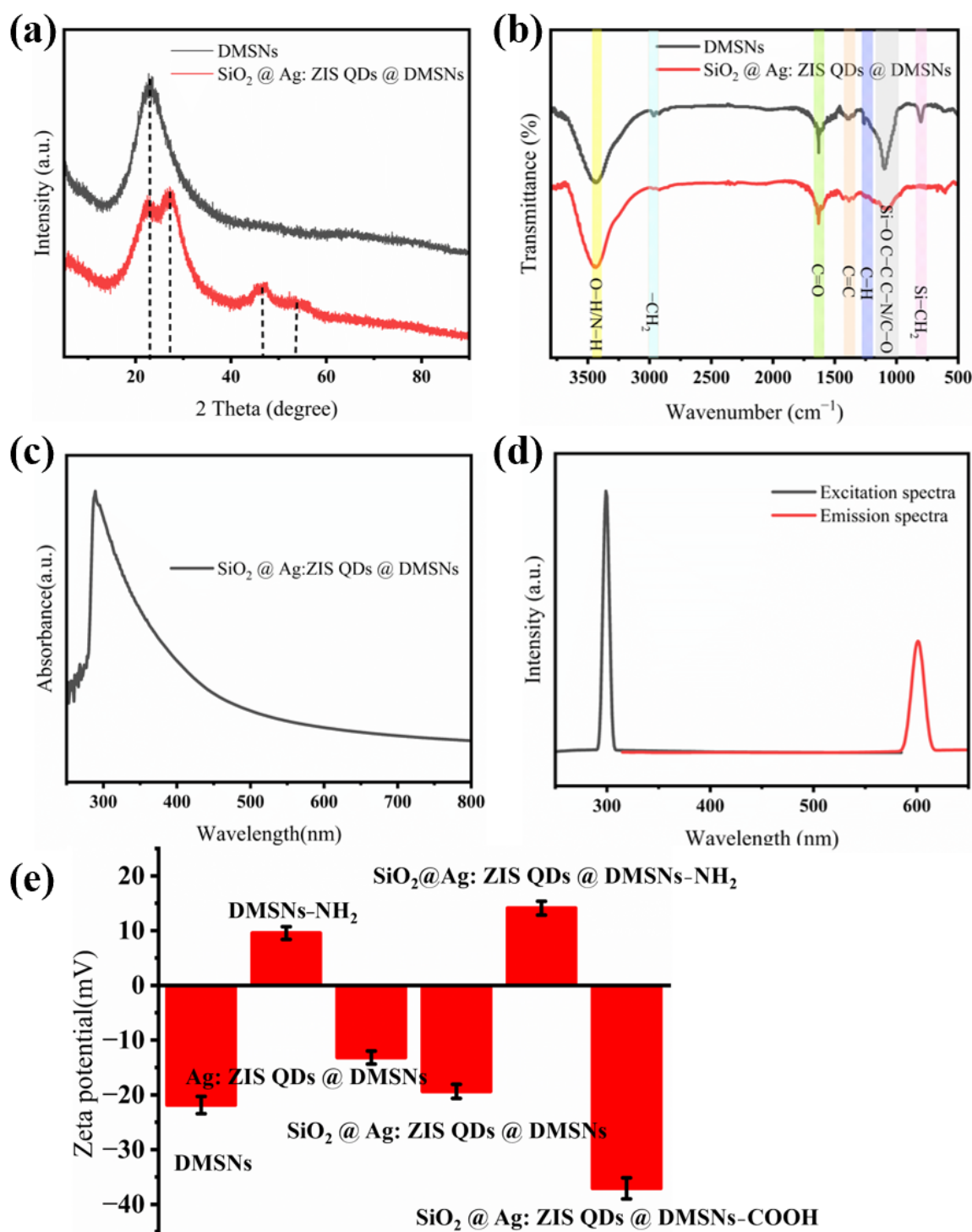


Figure 4. (a) XRD of DMSNs and SiO₂ @ Ag: ZIS QDs @ DMSNs; (b) FT-IR spectra of DMSNs and SiO₂ @ Ag: ZIS QDs @ DMSNs; (c) UV-vis absorption spectra of SiO₂ @ Ag: ZIS QDs @ DMSNs; (d) fluorescence emission spectra and excitation spectra of SiO₂ @ Ag: ZIS QDs @ DMSNs; (e) ζ -potential of DMSNs, DMSNs-NH₂, SiO₂ @ Ag: ZIS QDs @ DMSNs, SiO₂ @ Ag: ZIS QDs @ DMSNs-NH₂, and SiO₂ @ Ag: ZIS QDs @ DMSNs-COOH.

3.2. Optimization of the Preparation of Ag: ZIS QDs @ DMSNs

Due to the novelty of the Ag: ZIS QDs @ DMSNs composite material being the first successful preparation of Ag: ZIS QDs combined with DMSNs, it is necessary to explore the impact of the amount of Ag: ZIS QDs on the fluorescence intensity and investigate

the optimal ratio of Ag: ZIS QDs to DMSNs. Different volumes (30, 50, 60, 70, 80 μL) of Ag: ZIS QDs aqueous solution add 10 mg of DMSNs, and the fluorescence intensity of the resulting composite materials is shown in Figure S2. The results indicate that the fluorescence intensity of Ag: ZIS QDs @ DMSNs is maximized when adding 50 μL of Ag: ZIS QDs aqueous solution. The fluorescence intensity decreases when the amount of Ag: ZIS QDs is below or above 50 μL . When the addition amount of quantum dots exceeds 50 μL , adhesion is likely to occur between composite nanospheres, leading to the aggregation of nanospheres and thus their inability to be applied in LFIA. Therefore, centrifugation and screening are performed after adhesion occurs, resulting in a decrease in fluorescence intensity. Therefore, the group with the most vigorous fluorescence intensity was selected as the signaling material to achieve susceptible and rapid detection of IBV. As shown in Figure S2, SiO_2 @ Ag: ZIS QDs @ DMSNs exhibits bright orange fluorescence under 365 nm ultraviolet light, demonstrating excellent water solubility and providing a stable foundation for subsequent detection. The orange fluorescence helps eliminate interference caused by the blue fluorescence background. Thus, from the perspective of fluorescence color, using SiO_2 @ Ag: ZIS QDs @ DMSNs as a signaling material significantly enhances detection sensitivity. To further explore the stability of SiO_2 @ Ag: ZIS QDs @ DMSNs composite material, we assessed its signal intensity stability at different pH values (ranging from 2 to 12). As shown in Figures S3 and S4, SiO_2 @ Ag: ZIS QDs @ DMSNs exhibits good stability in acidic and alkaline solutions, whereas Ag: ZIS QDs @ DMSNs shows poor acid-alkali resistance. This significant improvement in pH stability is attributed to the unique surface characteristics of the silica shell. Additionally, we evaluated the signal intensity stability of SiO_2 @ Ag: ZIS QDs @ DMSNs under long-term storage conditions. The results indicate that the fluorescence intensity of SiO_2 @ Ag: ZIS QDs @ DMSNs is hardly affected by time, meeting the requirements of LFIA (Figure S5).

3.3. Rapid and Sensitive Detection of IBV Using LFIA Test Strips Based on SiO_2 @ Ag: ZIS QDs @ DMSNs

The detection principle is based on a direct detection format using the sandwich immunoassay, where the target antigen is captured between the capture antibody on the detector and the test system. The process begins with binding the fluorescent signal moiety to the target IBV protein. An immune complex is formed after the conjugate interacts with the target antigen. This immune complex flows through the NC membrane due to capillary force, and it is captured at the T line position and composed of captured mAbB molecules. The formation of the sandwich complex causes particle aggregation at the T line, enabling the observation of the fluorescent detection signal. Excess and unbound conjugates then migrate past the C line, where goat anti-mouse IgG antibodies capture them to validate the accuracy of the device's operation. This three-layered sandwich immunoassay provides a direct and efficient method for detecting the target protein in the context of IBV, enhancing the sensitivity and specificity of the diagnostic system [37].

Based on the excellent fluorescent properties, stability, and dispersibility of SiO_2 @ Ag: ZIS QDs @ DMSNs, we employed them as fluorescent signal molecules, coupled with IBV-Ab₂, for the specific detection of IBV antigen in LFIA format. As shown in Figure 5a, in the presence of the target analyte (IBV), the sandwich immune reaction selectively captures the SiO_2 @ Ag: ZIS QDs @ DMSNs antibody conjugate on the test line, generating a positive fluorescent signal. Conversely, the absence of SiO_2 @ Ag: ZIS QDs @ DMSNs fluorescence on the test line indicates the absence of the target antigen in the sample, resulting in a negative result. In both cases (presence and absence of antigen), the goat anti-mouse IgG antibody that is immobilized on the control line binds to the anti-IBV-Ab₂ that is conjugated to the SiO_2 @ Ag: ZIS QDs @ DMSNs. The test strips were visualized using a 365 nm UV lamp. The quantitative concentration of the analyte in the sample was further determined by calculating the ratio of the fluorescence intensity of the test line to the control line (T/C).

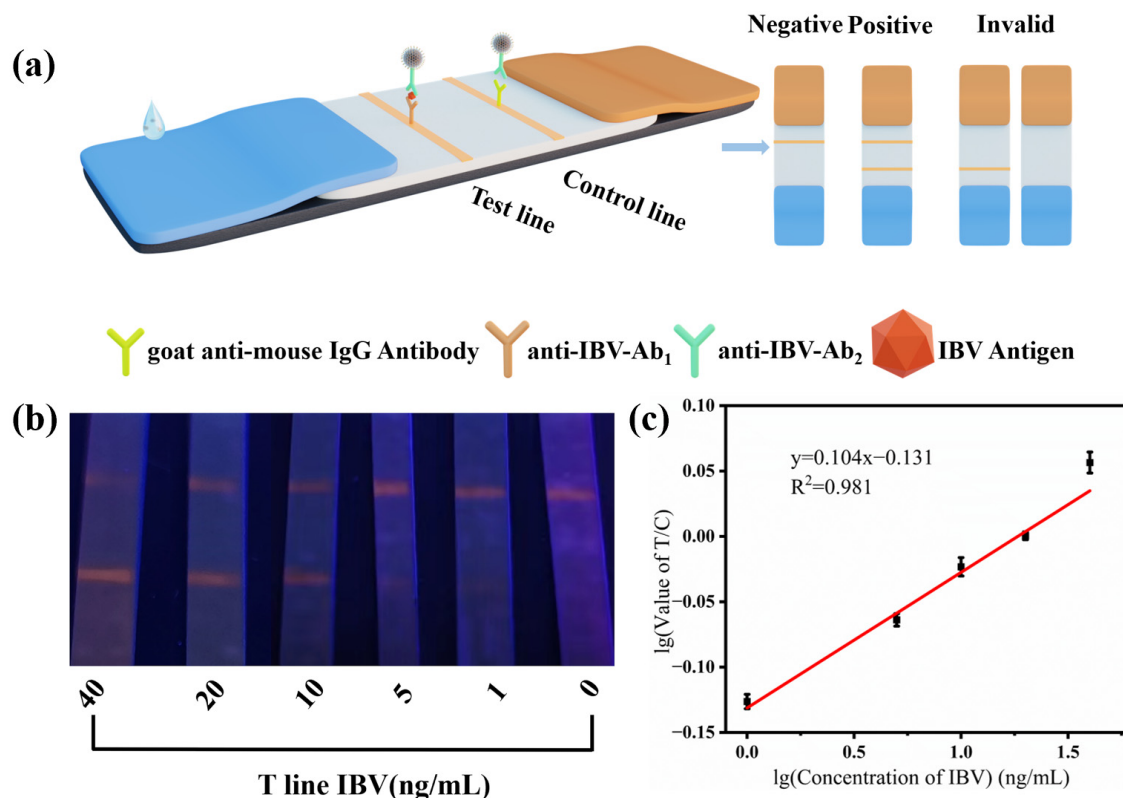


Figure 5. (a) The detection process of IBV using $\text{SiO}_2 @ \text{Ag}: \text{ZIS QDs} @ \text{DMSNs}$; (b) the picture of the $\text{SiO}_2 @ \text{Ag}: \text{ZIS QDs} @ \text{DMSNs}$ -LFIA detecting different concentrations of IBV solutions; (c) linear response of the $\text{SiO}_2 @ \text{Ag}: \text{ZIS QDs} @ \text{DMSNs}$ -LFIA to IBV detection, with a concentration range of $40 \text{ ng/mL}^{-1} \text{ ng/mL}$.

Different concentrations (0, 1, 5, 10, 20, 40 ng/mL) of IBV antigen standard solutions were analyzed using $\text{SiO}_2 @ \text{Ag}: \text{ZIS QDs} @ \text{DMSNs}$ -LFIA to assess sensitivity. The results of the test paper were analyzed using a Huawei smartphone, as shown in Figure 5b. All control lines on the test strips exhibited fluorescent signals, indicating the validity of the test results. The results demonstrated an LOD of approximately 1 ng/mL for IBV. $\text{SiO}_2 @ \text{Ag}: \text{ZIS QDs} @ \text{DMSNs}$ -LFIA fully utilized the high orange fluorescence intensity of $\text{Ag}: \text{ZIS QDs}$, effectively lowering the detection limit. The signal intensity of the T and C lines was quantified using ImageJ software. The relationship between the brightness of the T line analyzed by ImageJ software and IBV concentration was represented by $y = 0.104x - 0.131$ ($R^2 = 0.981$), as shown in Figure 5c.

In addition, we conducted a thorough investigation on the stability of $\text{SiO}_2 @ \text{Ag}: \text{ZIS QDs} @ \text{DMSNs}$ -LFIA. By placing the labeled antibody conjugate for different durations and then applying it to the test strip for testing, we found that its biological activity did not decrease significantly. As shown in Figure S6, even after a period of storage, the labeled antibody conjugate can still maintain good fluorescence signals and detection performance. This result fully demonstrates that the $\text{SiO}_2 @ \text{Ag}: \text{ZIS QDs} @ \text{DMSNs}$ -LFIA test strip has excellent stability and can maintain stable detection performance under different conditions.

Evaluating the intra- and inter-assay CV is fundamental for accurately identifying the target analyte using $\text{SiO}_2 @ \text{Ag}: \text{ZIS QDs} @ \text{DMSNs}$ -LFIA. The precision of $\text{SiO}_2 @ \text{Ag}: \text{ZIS QDs} @ \text{DMSNs}$ -LFIA was assessed using a standard solution containing 100 ng/mL IBV antigen. Intra- and inter-batch measurements were performed in quintuplicate. As shown in Table S1, both intra and inter-assay CVs were below 9%, indicating that $\text{SiO}_2 @ \text{Ag}: \text{ZIS QDs} @ \text{DMSNs}$ -LFIA exhibited highly satisfactory accuracy. Additionally, the specificity of $\text{SiO}_2 @ \text{Ag}: \text{ZIS QDs} @ \text{DMSNs}$ -LFIA was validated by assessing three biomarkers, Zika virus (ZIKA), alpha-fetoprotein (AFP), and human chorionic gonadotropin (HCG), at a

concentration of 1 $\mu\text{g}/\text{mL}$. As depicted in Figure 6, except for IBV, no orange fluorescence was observed on the test line for the other three biomarkers, demonstrating the excellent selectivity of $\text{SiO}_2 @ \text{Ag}: \text{ZIS QDs} @ \text{DMSNs-LFIA}$. Furthermore, Table S2 presents a comparative analysis of the analytical performance of diverse methods for IBV detection. $\text{SiO}_2 @ \text{Ag}: \text{ZIS QDs} @ \text{DMSNs-LFIA}$ offers the advantages of rapidity and convenience. When compared to fluorescence sensing methods, $\text{SiO}_2 @ \text{Ag}: \text{ZIS QDs} @ \text{DMSNs-LFIA}$ exhibits a lower LOD than colloidal gold test strip, and is more portable and cost-effective, thus demonstrating excellent application value.

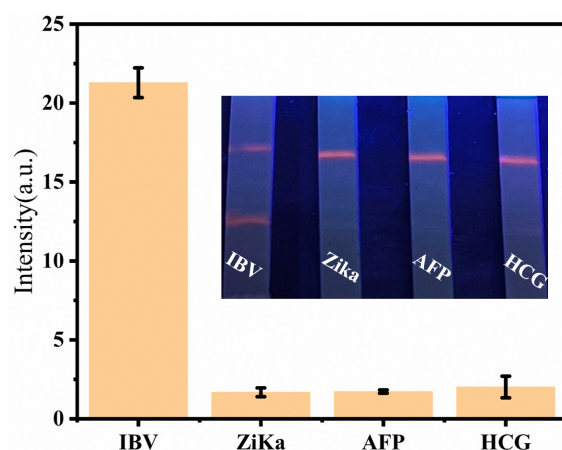


Figure 6. Study on the specificity of $\text{SiO}_2 @ \text{Ag}: \text{ZIS QDs} @ \text{DMSNs-LFIA}$ test strip to different interfering proteins.

4. Conclusions

In summary, we have developed a $\text{SiO}_2 @ \text{Ag}: \text{ZIS QDs} @ \text{DMSNs}$ -based LFIA that is simple, sensitive, and specific. This innovative material exhibits orange fluorescence, which could effectively mitigate background fluorescence interference commonly encountered in test strips. The developed sensor facilitates rapid detection, is capable of delivering results within a brief period of 10 min, and is characterized by its ease of operation, demanding a minimal sample volume of just 30 μL . Furthermore, the biosensor demonstrates a detection limit for IBV of 1 ng/mL, significantly surpassing conventional colloidal gold strips. The resultant sensor enables rapid detection and is user-friendly, requiring only 30 μL of sample. Furthermore, the biosensor demonstrates a detection limit for IBV of 1 ng/mL, significantly surpassing conventional colloidal gold strips. Our research not only advances influenza detection, but also lays the groundwork for the development of highly sensitive and adaptable diagnostic tools.

Supplementary Materials: The following supporting information can be downloaded at <https://www.mdpi.com/article/10.3390/chemosensors12040068/s1>, Figure S1. (a) TEM images of DMSNs and the corresponding particle size distribution (inset); (b) TEM image of $\text{Ag}: \text{ZIS QDs} @ \text{DMSNs}$; (c) TEM image of $\text{SiO}_2 @ \text{Ag}: \text{ZIS QDs} @ \text{DMSNs}$; (d) EDS mapping images of $\text{SiO}_2 @ \text{Ag}: \text{ZIS QDs} @ \text{DMSNs}$; Figure S2: The effect of QDs addition amount on the fluorescence properties of $\text{SiO}_2 @ \text{Ag}: \text{ZIS QDs} @ \text{DMSNs}$ (the inset is the fluorescence photos of $\text{SiO}_2 @ \text{Ag}: \text{ZIS QDs} @ \text{DMSNs}$); Figure S3: Photos of $\text{Ag}: \text{ZIS QDs} @ \text{DMSNs}$ aqueous solutions at different pH values under a 365 nm fluorescent lamp; Figure S4: Photos of $\text{SiO}_2 @ \text{Ag}: \text{ZIS QDs} @ \text{DMSNs}$ aqueous solutions at different pH values under a 365 nm fluorescent lamp; Figure S5: Fluorescence signal intensity of $\text{SiO}_2 @ \text{Ag}: \text{ZIS QDs} @ \text{DMSNs}$ under long-term storage; Figure S6: Study on the Stability of $\text{SiO}_2 @ \text{Ag}: \text{ZIS QDs} @ \text{DMSNs-LFIA}$; Table S1: The results of the CV of $\text{SiO}_2 @ \text{Ag}: \text{ZIS QDs} @ \text{DMSNs-LFIA}$ (IBV); Table S2: Summary of IBV detection with some different detection methods. Reference [38] is cited in the Supplementary Materials

Author Contributions: Conceptualization, S.-N.D.; Methodology, J.-X.H. and S.-N.D.; Validation, J.-X.H.; Investigation, J.-X.H., L.-B.Z. and S.-T.W.; Resources, S.-N.D.; Data Curation, J.-X.H.; Writing—

Original Draft Preparation, J.-X.H.; Writing—Review and Editing, J.-X.H., L.-B.Z., S.-T.W. and S.-N.D.; Visualization, J.-X.H.; Supervision, S.-N.D.; Project Administration, S.-N.D.; Funding Acquisition, S.-N.D. All authors have read and agreed to the published version of the manuscript.

Funding: This work was supported by the National Natural Science Foundation of China (21575022), and the National Key Research and Development Program of China (2017YFA0700404).

Institutional Review Board Statement: Not applicable.

Informed Consent Statement: Not applicable.

Data Availability Statement: The data presented in this study are available on request from the corresponding author.

Conflicts of Interest: The authors declare no conflicts of interest.

References

1. Su, S.; Chaves, S.S.; Perez, A.; D’Mello, T.; Kirley, P.D.; Yousey-Hindes, K.; Farley, M.M.; Harris, M.; Sharangpani, R.; Lynfield, R.; et al. Comparing clinical characteristics between hospitalized adults with laboratory-confirmed influenza A and B virus infection. *Clin. Infect. Dis.* **2014**, *59*, 252–255. [[CrossRef](#)] [[PubMed](#)]
2. Chan, P.K.S.; Chan, M.C.W.; Cheung, J.L.K.; Lee, N.; Leung, T.F.; Yeung, A.C.M.; Wong, M.C.S.; Ngai, K.L.K.; Nelson, E.A.S.; Hui, D.S.C. Influenza B lineage circulation and hospitalization rates in a subtropical city, Hong Kong, 2000–2010. *Clin. Infect. Dis.* **2013**, *56*, 677–684. [[CrossRef](#)] [[PubMed](#)]
3. Paddock, C.D.; Liu, L.; Denison, A.M.; Bartlett, J.H.; Holman, R.C.; Deleon-Carnes, M.; Emery, S.L.; Drew, C.P.; Shieh, W.J.; Uyeki, T.M.; et al. Myocardial injury and bacterial pneumonia contribute to the pathogenesis of fatal influenza B virus infection. *J. Infect. Dis.* **2012**, *205*, 895–905. [[CrossRef](#)] [[PubMed](#)]
4. Liang, J.; Wu, L.; Wang, Y.; Liang, W.; Hao, Y.; Tan, M.; He, G.; Lv, D.; Wang, Z.; Zeng, T.; et al. SERS/photothermal-based dual-modal lateral flow immunoassays for sensitive and simultaneous antigen detection of respiratory viral infections. *Sensors Actuators B Chem.* **2023**, *389*, 133875. [[CrossRef](#)]
5. Duev-Cohen, A.; Isaacson, B.; Berhani, O.; Charpak-Amikam, Y.; Friedman, N.; Drori, Y.; Mandelboim, M.; Mandelboim, O. Altered Nkp46 recognition and elimination of influenza B viruses. *Viruses* **2021**, *13*, 34. [[CrossRef](#)] [[PubMed](#)]
6. Asif, M.; Xu, Y.; Xiao, F.; Sun, Y. Diagnosis of COVID-19, vitality of emerging technologies and preventive measures. *Chem. Eng. J.* **2021**, *423*, 130189. [[CrossRef](#)] [[PubMed](#)]
7. Han, M.S.; Byun, J.H.; Cho, Y.; Rim, J.H. RT-PCR for SARS-CoV-2: Quantitative versus qualitative. *Lancet Infect. Dis.* **2021**, *21*, 165. [[CrossRef](#)] [[PubMed](#)]
8. Madadelahi, M.; Agarwal, R.; Martinez-Chapa, S.O.; Madou, M.J. A roadmap to high-speed polymerase chain reaction (PCR): COVID-19 as a technology accelerator. *Biosens. Bioelectron.* **2024**, *246*, 115830. [[CrossRef](#)]
9. Baldofski, S.; Hoffmann, H.; Lehmann, A.; Breitfeld, S.; Garbe, L.A.; Schneider, R.J. Enzyme-linked immunosorbent assay (ELISA) for the anthropogenic marker is lithocholic acid in water. *J. Environ. Manag.* **2016**, *182*, 612–619. [[CrossRef](#)]
10. Zhang, Y.; Zhao, S.; Zheng, J.; He, L. Surface-enhanced Raman spectroscopy (SERS) combined techniques for high-performance detection and characterization. *TrAC Trends Anal. Chem.* **2017**, *90*, 1–13. [[CrossRef](#)]
11. Hu, J.X.; Ding, S.N. In situ synthesis of highly fluorescent, phosphorus-doping carbon-dot-functionalized, dendritic silica nanoparticles applied for multi-component lateral flow immunoassay. *Sensors* **2023**, *24*, 19. [[CrossRef](#)] [[PubMed](#)]
12. Zong, H.; Zhang, S.; Shang, X.; Jiang, H.; Zhao, Z.; Chen, S.; Wang, X.; Wang, Y.; Jiang, Y.; Li, X.; et al. Development of an AlphaLISA assay for sensitive and accurate detection of influenza B virus. *Front. Med.* **2023**, *10*, 1155551. [[CrossRef](#)]
13. Wu, W.; Li, M.; Chen, M.; Li, L.; Wang, R.; Chen, H.; Chen F.; Mi, Q.; Liang, W.; Chen, H. Development of a colloidal gold immunochromatographic strip for rapid detection of *Streptococcus agalactiae* in tilapia. *Biosens. Bioelectron.* **2017**, *91*, 66–69. [[CrossRef](#)] [[PubMed](#)]
14. Wu, Y.; Wu, M.; Liu, C.; Tian, Y.; Fang, S.; Yang, H.; Li, B.; Liu, Q. Colloidal gold immunochromatographic test strips for broad-spectrum detection of *Salmonella*. *Food Control* **2021**, *126*, 108052. [[CrossRef](#)]
15. Yao, Y.; Zou, M.; Wu, H.; Ma, S.; Gu, X.; Zhou, M.; Zhao, F.; Abudushalamua, G.; Xiao, F.; Chen, Y.; et al. A colloidal gold test strip based on catalytic hairpin assembly for the clinical detection of influenza A virus nucleic acid. *Talanta* **2023**, *265*, 124855. [[CrossRef](#)]
16. Wang, Y.; Wang, T.; Wang, M.; Wang, J.; Xu, Z.; Zhang, H. Photothermal card reader assay using the commercial colloidal gold test strip for the rapid quantitative detection of food hazards. *Mikrochim. Acta* **2022**, *189*, 112. [[CrossRef](#)]
17. Huang, D.; Lin, B.; Song, Y.; Guan, Z.; Cheng, J.; Zhu, Z.; Yang, C. Staining traditional colloidal gold test strips with Pt nanoshell enables quantitative point-of-care testing with simple and portable pressure meter readout. *ACS Appl. Mater. Interfaces* **2019**, *11*, 1800–1806. [[CrossRef](#)]
18. Moon, H.; Lee, C.; Lee, W.; Kim, J.; Chae, H. Stability of quantum dots, quantum dot films, and quantum dot light-emitting diodes for display applications. *Adv. Mater.* **2019**, *31*, 14. [[CrossRef](#)]
19. Foubert, A.; Beloglazova, N.V.; De Saeger, S. Comparative study of colloidal gold and quantum dots as labels for multiplex screening tests for multi-mycotoxin detection. *Anal. Chim. Acta* **2017**, *955*, 48–57. [[CrossRef](#)]

20. Jang, G.; Jo, D.Y.; Ma, S.; Lee, J.; Son, J.; Lee, C.U.; Jeong, W.; Yang, S.; Park, J.H.; Yang, H.; et al. Core-shell perovskite quantum dots for highly selective room-temperature spin light-emitting diodes. *Adv. Mater.* **2024**, *36*, e2309335. [[CrossRef](#)]
21. Fang, B.; Xiong, Q.; Duan, H.; Xiong, Y.; Lai, W. Tailored quantum dots for enhancing sensing performance of lateral flow immunoassay. *TrAC Trends Anal. Chem.* **2022**, *157*, 116754. [[CrossRef](#)]
22. Gao, F.; Liu, C.; Yao, Y.; Lei, C.; Li, S.; Yuan, L.; Song, H.; Yang, Y.; Wan, J.; Yu, C. Quantum dots' size matters for balancing their quantity and quality in label materials to improve lateral flow immunoassay performance for C-reactive protein determination. *Biosens. Bioelectron.* **2022**, *199*, 113892. [[CrossRef](#)] [[PubMed](#)]
23. Chen, J.; Jiang, J.; Liang, J.; Wu, H.; Chen, L.; Xu, Z.; Lei, H.; Li, X. Bifunctional magnetic ZnCdSe/ZnS quantum dots nanocomposite-based lateral flow immunoassay for ultrasensitive detection of streptomycin and dihydrostreptomycin in milk, muscle, liver, kidney, and honey. *Food Chem.* **2023**, *406*, 135022. [[CrossRef](#)] [[PubMed](#)]
24. Li, H.; Dong, B.; Dou, L.; Yu, W.; Yu, X.; Wen, K.; Ke, Y.; Shen, J.; Wang, Z. Fluorescent lateral flow immunoassay for highly sensitive detection of eight anticoagulant rodenticides based on cadmium-free quantum dot-encapsulated nanospheres. *Sens. Actuators B Chem.* **2020**, *324*, 128771. [[CrossRef](#)]
25. Rong, Z.; Bai, Z.; Li, J.; Tang, H.; Shen, T.; Wang, Q.; Wang, C.; Xiao, R.; Wang, S. Dual-color magnetic-quantum dot nanobeads as versatile fluorescent probes in test strip for simultaneous point-of-care detection of free and complexed prostate-specific antigen. *Biosens. Bioelectron.* **2019**, *145*, 111719. [[CrossRef](#)] [[PubMed](#)]
26. Wang, N.; Liu, Z.X.; Li, R.S.; Zhang, H.Z.; Huang, C.Z.; Wang, J. The aggregation-induced emission quenching of graphene quantum dots for visualizing the dynamic invasions of cobalt(ii) into living cells. *J. Mater. Chem. B* **2017**, *5*, 6394–6399. [[CrossRef](#)] [[PubMed](#)]
27. Kim, K.S.; Zakia, M.; Yoon, J.; Yoo, S.I. Metal-enhanced fluorescence in polymer composite films with Au @ Ag@SiO₂ nanoparticles and InP@ZnS quantum dots. *RSC Adv.* **2018**, *9*, 224–233. [[CrossRef](#)] [[PubMed](#)]
28. Li, J.; Lv, Y.; Li, N.; Wu, R.; Xing, M.; Shen, H.; Li, L.S.; Chen, X. Robust synthesis of bright multiple quantum dot-embedded nanobeads and its application to quantitative immunoassay. *Chem. Eng. J.* **2019**, *361*, 499–507. [[CrossRef](#)]
29. Ezhov, A.A.; Karpov, O.N.; Merkalov, A.S.; Abramchuk, S.S.; Bondarenko, G.N.; Talroze, R.V. Quantum dots—Polymer composites and the influence of gold nanoparticles on photoluminescence of polymer composite films. *J. Lumin.* **2020**, *220*, 116992. [[CrossRef](#)]
30. Li, C.; Zou, Z.; Liu, H.; Jin, Y.; Li, G.; Yuan, C.; Xiao, Z.; Jin, M. Synthesis of polystyrene-based fluorescent quantum dots nanolabel and its performance in H5N1 virus and SARS-CoV-2 antibody sensing. *Talanta* **2021**, *225*, 122064. [[CrossRef](#)]
31. Wang, C.; Yang, X.; Zheng, S.; Cheng, X.; Xiao, R.; Li, Q.; Wang, W.; Liu, X.; Wang, S. Development of an ultrasensitive fluorescent immunochromatographic assay based on multilayer quantum dot nanobead for simultaneous detection of SARS-CoV-2 antigen and influenza A virus. *Sens. Actuators B Chem.* **2021**, *345*, 130372. [[CrossRef](#)]
32. Liu, H.; Cao, J.; Ding, S.N. Simultaneous detection of two ovarian cancer biomarkers in human serums with biotin-enriched dendritic mesoporous silica nanoparticles-labeled multiplex lateral flow immunoassay. *Sens. Actuators B Chem.* **2022**, *371*, 132597. [[CrossRef](#)]
33. Gao, F.; Lei, C.; Liu, Y.; Song, H.; Kong, Y.Q.; Wan, J.J.; Yu, C.Z. Rational design of dendritic mesoporous silica nanoparticles' surface chemistry for quantum dot enrichment and an ultrasensitive lateral flow immunoassay. *ACS Appl. Mater. Interfaces* **2021**, *13*, 21507–21515. [[CrossRef](#)]
34. Zhu, L.B.; Ding, S.N. Enhancing the photocatalytic performance of antibiotics using a Z-Scheme heterojunction of 0D ZnIn₂S₄ quantum dots and 3D hierarchical inverse opal TiO₂. *Molecules* **2023**, *28*, 7174. [[CrossRef](#)]
35. Xu, L.D.; Zhu, J.; Ding, S.N. Highly-fluorescent carbon dots grown onto dendritic silica nanospheres for anthrax protective antigen detection. *Anal. Methods* **2022**, *14*, 1836–1840. [[CrossRef](#)]
36. Valdman, L.; Mazánek, V.; Marvan, P.; Serra, M.; Arenal, R.; Sofer, Z. Layered ZnIn₂S₄ single crystals for ultrasensitive and wearable photodetectors. *Adv. Opt. Mater.* **2021**, *9*, 2100845. [[CrossRef](#)]
37. Yin, X.; Liu, S.; Kukkar, D.; Wang, J.; Zhang, D.; Kim, K.-H. Performance enhancement of the lateral flow immunoassay by use of composite nanoparticles as signal labels. *TrAC Trends Anal. Chem.* **2024**, *170*, 117441. [[CrossRef](#)]
38. Raji, M.A.; Aloraij, Y.; Alhamlan, F.; Suaifan, G.; Weber, K.; Cialla-May, D.; Popp, J.; Zourob, M. Development of rapid colorimetric assay for the detection of Influenza A and B viruses. *Talanta* **2021**, *221*, 121468. [[CrossRef](#)]

Disclaimer/Publisher's Note: The statements, opinions and data contained in all publications are solely those of the individual author(s) and contributor(s) and not of MDPI and/or the editor(s). MDPI and/or the editor(s) disclaim responsibility for any injury to people or property resulting from any ideas, methods, instructions or products referred to in the content.